Research Article

Nano Research
2023, 16(7): 10436–10442

ISSN 1998-0124 CN 11-5974/O4
https://doi.org/10.1007/s12274-023-5605-2

On-surface synthesis and edge states of NBN-doped zigzag graphene nanoribbons

Xiao Chang[1,2,§], Li Huang[1,2,§], Yixuan Gao[1,2,§], Yubin Fu[3,4,§], Ji Ma[3,4], Huan Yang[1,2], Junzhi Liu[5], Xiaoshuai Fu[1,2], Xiao Lin[1,2] (✉), Xinliang Feng[3,4] (✉), Shixuan Du[1,2,6] (✉), and Hong-Jun Gao[1,2,6] (✉)

[1] *University of Chinese Academy of Sciences, Beijing 100190, China*
[2] *Beijing National Center for Condensed Matter Physics, Institute of Physics, Chinese Academy of Sciences, Beijing 100190, China*
[3] *Center for Advancing Electronics Dresden (CfAED) and Faculty of Chemistry and Food Chemistry, Technische Universität Dresden, Dresden D-01069, Germany*
[4] *Max Planck Institute of Microstructure Physics, Weinberg 2, Halle 06120, Germany*
[5] *Department of Chemistry, State Key Laboratory of Synthetic Chemistry, The University of Hong Kong, Hong Kong 999077, China*
[6] *Songshan Lake Materials Laboratory, Dongguan 523808, China*
[§] *Xiao Chang, Li Huang, Yixuan Gao, and Yubin Fu contributed equally to this work.*

Received: 24 December 2022 / **Revised:** 13 February 2023 / **Accepted:** 22 February 2023

ABSTRACT

Zigzag graphene nanoribbons (ZGNRs) with spin-polarized edge states have potential applications in carbon-based spintronics. The electronic structure of ZGNRs can be effectively tuned by different widths or dopants, which requires delicately designed monomers. Here, we report the successful synthesis of ZGNR with a width of eight carbon zigzag lines and nitrogen-boron-nitrogen (NBN) motifs decorated along the zigzag edges (NBN-8-ZGNR) on Au (111) surface, which starts from a specially designed U-shaped monomer with preinstalled NBN units at the zigzag edge. Chemical-bond-resolved non-contact atomic force microscopy (nc-AFM) imaging confirms the zigzag-terminated edges and the existence of NBN dopants. The electronic states distributed along the zigzag edges have been revealed after a silicon-layer intercalation at the interface of NBN-8-ZGNR and Au (111). Our work enriches the ZGNR family with a new dopant and larger width, which provides more candidates for future carbon-based nanoelectronic and spintronic applications.

KEYWORDS

zigzag graphene nanoribbons, nitrogen-boron-nitrogen (NBN) dopant, edge states, scanning tunneling microscopy (STM), non-contact atomic force microscopy (nc-AFM), density functional theory (DFT) calculations

1 Introduction

Graphene nanoribbons (GNRs) are renowned for their fascinating electronic and magnetic properties, which have potential applications in carbon-based nanoelectronics and spintronics [1]. The edge configurations of GNRs greatly influence their electronic structures [2], thus atomically precise synthetic methods are needed to construct GNRs with designed properties. Surface-assistant fabrication starting with organic precursors has been proven to be a powerful bottom–up approach to synthesize specifically designed graphene nanostructures [3–10]. Up to now, a variety of GNRs have been synthesized on surface, including GNRs with armchair- [9, 11–13], zigzag- [4, 14], and chevron-terminated edges [15–17], with dopants of nitrogen [18, 19], boron [11–13, 20], and sulfur atoms [15, 21, 22], and heterostructures splicing with different widths [6–8, 23, 24] or edges [25–27].

Zigzag GNRs (ZGNRs) host spin-polarized electronic edge states [2], which are ideal prototype materials to explore carbon-based spintronics and qubits [28–30]. The spin-polarized edge states are anti-ferromagnetic on opposite edges of ZGNRs, which, however, is difficult to be directly observed due to a strong hybridization with the underlying metal substrate [4]. Moreover, the zigzag edges constructed with all carbon atoms are highly reactive [31, 32], hindering their further exploration. An effective strategy to decouple the zigzag edges from the substrate is to introduce a superlattice of isoelectronic dopants along the edges, such as nitrogen atoms and nitrogen-boron-nitrogen (NBN) motifs [14, 33]. An N-doped 6-ZGNR has recently been demonstrated to successfully stabilize the edges and electronically decouple the spin-polarized edge states from hybridization with the substrate [14]. The NBN dopants have been predicted not only to have the ability to stabilize the edges [34], but also to enable the formation of radical cation by selective oxidation [35], which is the isoelectronic structure of its all-carbon skeleton with an open-shell character. NBN-doped partial ZGNRs with cove features were synthesized in 2020 by us [33], in which the spin-polarized edge states are absent due to the short length of continuous zigzag edges. Therefore, to investigate the spin-polarized electronic edge states, a full ZGNR with NBN-doped superlattice along the edges will be a potential candidate.

Address correspondence to Hong-Jun Gao, hjgao@iphy.ac.cn; Shixuan Du, sxdu@iphy.ac.cn; Xinliang Feng, xinliang.feng@tu-dresden.de; Xiao Lin, xlin@ucas.ac.cn

清華大學出版社 Tsinghua University Press Springer

Here, we designed and synthesized a U-shaped precursor with an interior isopropyl-diphenyl group, 4,13-bis(4-iodophenyl)-2-(4'-isopropyl-[1,1'-biphenyl]-4-yl)-8*H*,9*H*-8,9-diaza-8a-borabenzo[*fg*]tetracene (BDBT, shown in Fig. 1(a)), which will yield ZGNR with eight carbon zigzag lines in width and NBN motifs along the edges (NBN-8-ZGNR). Subsequent deposition of BDBT molecules on Au (111) surface followed by annealing demonstrates the formation of NBN-8-ZGNRs. Using non-contact atomic force microscopy (nc-AFM), we confirmed the structures of the NBN-8-ZGNRs and their purely zigzag edges. By silicon intercalation [36–38], a gold silicide (AuSIL) buffer layer [39] was created between Au and NBN-ZGNRs, which effectively decouples the surface states of Au (111) and enables the measurement of the electronic states of the NBN-ZGNRs. Localized states are detected on the zigzag edges, which indicates the edge states are preserved on NBN-doped zigzag edges. Furthermore, the detection of the edge states demonstrates that NBN dopants make the zigzag edges less active and survive during the silicon intercalation process.

2 Results and discussion

The U-shaped BDBT monomer, which has an NBN-containing benzotetracene core with additional α, β, and γ benzene rings, an isopropyl group, and two halogen functions (Fig. 1(a)), was successfully obtained through multi-step solution-based chemical reactions as displayed in Scheme 1. First, by Suzuki reaction of (4-isopropylphenyl)boronic acid (compound 1) with (4-bromophenyl)trimethylsilane, (4'-isopropyl-[1,1'-biphenyl]-4-yl)trimethylsilane (compound 2) was obtained in 96% yield. Next, the trimethylsilyl (TMS) group in compound 2 was converted into boronic acid group by treatment with an excess of boron tribromide (BBr_3) followed by H_2O, which gave the (4'-isopropyl-[1,1'-biphenyl]-4-yl)boronic acid (compound 3) in 88% yield. Then a Suzuki reaction of compound 3 with 1,3-dibromo-5-iodobenzene afforded 3,5-dibromo-4"-isopropyl-1,1':4',1"-terphenyl (compound 4) in 91% yield. Afterward, 2,2'-(4"-isopropyl-[1,1':4',1"-terphenyl]-3,5-diyl)bis(4,4,5,5-tetramethyl-1,3,2-dioxaborolane) (compound 5) was generated in 73% yield via the Miyaura borylation reaction based on compound 4. A two-fold Suzuki reaction of compound 5 with 1-bromo-2-iodo-3-nitrobenzene afforded 2-bromo-5'-(2-bromo-6-nitrophenyl)-4'''-isopropyl-6-nitro-1,1':3',1":4",1'''-quaterphenyl (compound 6) in 58% yield. After another two-fold Suzuki reaction based on compound 6 and (4-(trimethylsilyl)phenyl)boronic acid, (5"-(4'-isopropyl-[1,1'-biphenyl]-4-yl)-3',6'''-dinitro-[1,1':2',1":3",1''':2''',1''''-quinquephenyl]-4,4''''-diyl)bis(trimethylsilane) (compound 7) was synthesized in 84% yield. Next, the TMS groups in compound 7 were converted into iodo groups by treatment with an excess of ICl, giving 4,4''''-diiodo-5"-(4'-isopropyl-[1,1'-biphenyl]-4-yl)-3',6'''-dinitro-1,1':2',1":3",1''':2''',1''''-quinquephenyl (compound 8) in 50% yield. Subsequently, compound 8 was reduced to 4,4''''-diiodo-5"-(4'-isopropyl-[1,1'-biphenyl]-4-yl)-[1,1':2',1":3",1''':2''',1''''-quinquephenyl]-3',6'''-diamine (compound 9) at room temperature (r.t.) in the presence of hydrogen gas with Pt/C in quantitative yield. Finally, heating of a solution of compound 9 in 1,2-dichlorobenzene (*o*-DCB) at 180 °C in the presence of BBr_3 with an excess of triethylamine (NEt_3) gave BDBT in 33% yield. The structure of BDBT was unambiguously confirmed by the nuclear magnetic resonance (NMR) spectroscopy (Figs. S24–S28 in the Electronic Supplementary Material (ESM)) and high-resolution matrix-assisted laser desorption/ionization time-of-flight (HR-MALDI-TOF) mass spectrometry (Fig. S29 in the ESM) after purification by silica column chromatography and subsequent recrystallization in $CHCl_3$/methanol (MeOH).

Starting from the BDBT monomer, the surface-assisted polymerization and subsequent cyclization enable the synthesis of

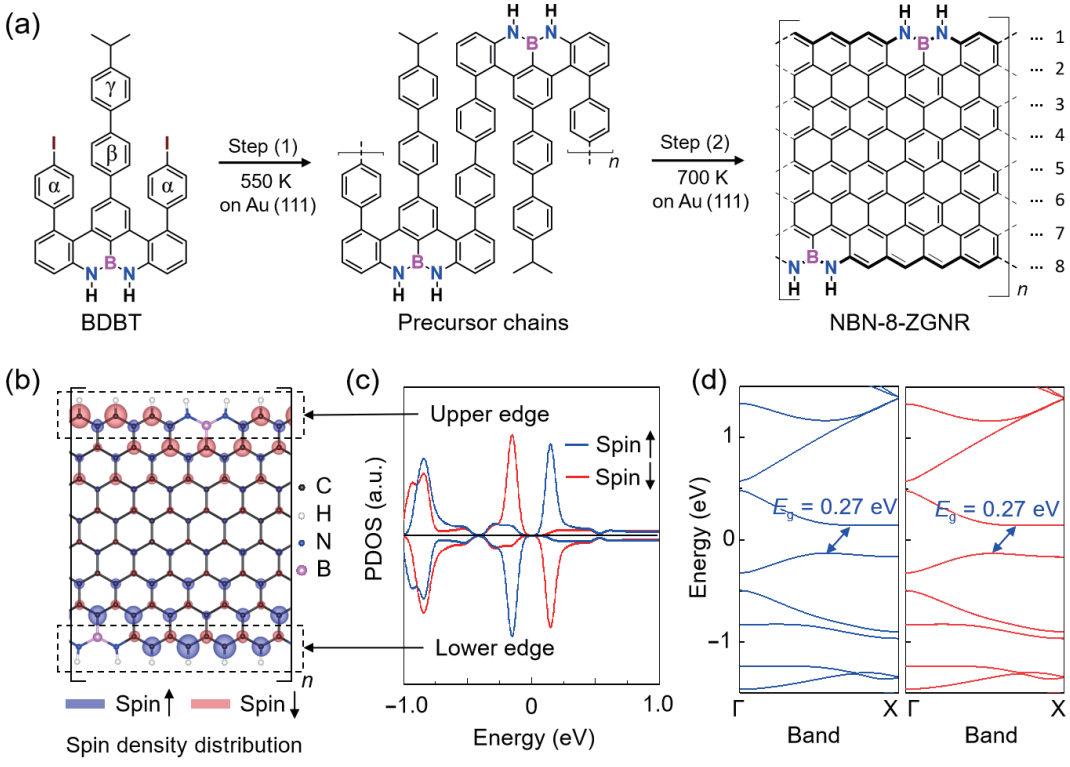

Figure 1 Synthetic process, DFT calculated band structure, and spatial distribution of spin-ordered edge states of NBN-8-ZGNRs. (a) Monomer BDBT, a U-shape monomer with an additional isopropyl-diphenyl group in the interior, is designed to synthesize NBN-8-ZGNRs through polymerization (step (1)) and subsequent cyclodehydrogenation (step (2)) on Au (111) surface. (b) DFT calculated spatial distribution of spin density in an NBN-8-ZGNR, in which the blue and coral circles denote the spin up and spin down states. (c) PDOS of the upper edge and lower edge atoms as marked by the black dashed boxes in (b). The blue and red lines indicate the spin up and spin down states. (d) DFT calculated band structure of a freestanding NBN-8-ZGNR. The blue and red lines indicate the spin up and spin down channels. The spin up and spin down states are degenerate.

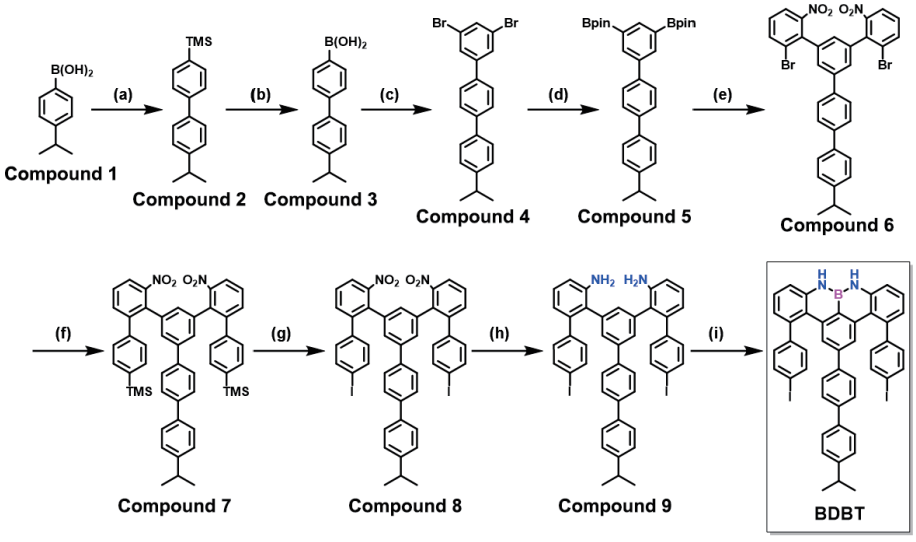

Scheme 1 Synthetic route to BDBT. Reagents and conditions: (a) (4-bromophenyl)trimethylsilane, $Pd(PPh_3)_4$, Cs_2CO_3, toluene, ethanol (EtOH), and H_2O, 80 °C, 12 h, 96%; (b) BBr_3, 100 °C, 4 h, then H_2O and n-hexane, 0 °C, 4 h, 88%; (c) 1,3-dibromo-5-iodobenzene, $Pd(PPh_3)_4$, Cs_2CO_3, toluene, EtOH, and H_2O, 80 °C, 12 h, 91%; (d) bis(pinacolato)diboron, $Pd(dppf)Cl_2$, KOAc, and dimethyl sulfoxide (DMSO), 100 °C, 24 h, 73%; (e) 1-bromo-2-iodo-3-nitrobenzene, $Pd(dppf)Cl_2$, Na_2CO_3, tetrahydrofuran (THF), and H_2O, 70 °C, 12 h, 58%; (f) (4-(trimethylsilyl)phenyl)boronic acid, $Pd(PPh_3)_4$, Cs_2CO_3, toluene, EtOH, and H_2O, 80 °C, 12 h, 84%; (g) ICl and dichloromethane (DCM), 0 °C–r.t., 12 h, 50%; (h) MeOH/THF, Pt/C, and H_2, r.t., 12 h, quantitative yield (crude); and (i) BCl_3, NEt_3, and *o*-DCB, 180 °C, 12 h, 30%.

NBN-8-ZGNRs on Au (111), as illustrated in Fig. 1(a). On the zigzag edges of NBN-8-ZGNRs, the NBN motifs insert in every six benzene rings, forming a superlattice of substitutional dopants along both edges. Density functional theory (DFT) calculations reveal that the NBN-8-ZGNRs, like other GNRs with zigzag edge topologies, have edge states that couple ferromagnetically along each edge and antiferromagnetically between the opposite edges (Fig. 1(b)). The spin-polarized edge states mainly distribute on the edge carbon atoms, but have little contribution from the substitutional dopants of NBN motifs. The projected density of states (PDOS) of the two edges are displayed in the upper and lower parts of Fig. 1(c), respectively. They are the density of states projected to the upper (lower) edge atoms as marked by the black dashed boxes in Fig. 1(b), which clearly demonstrate the spin-polarized nature of the edges. The DFT calculated band structure of a freestanding NBN-8-ZGNR in Fig. 1(d) shows that this ribbon has an indirect band gap of 0.27 eV, and the spin up and spin down states are degenerate in the ribbon.

The BDBT monomer was sublimed from a molecule cell evaporator at 530 K onto a clean Au (111) substrate held at room temperature in ultrahigh vacuum. The as-deposited monomers form linear or circular self-assemblies that are adsorbed respectively on the face centered cubic (fcc) and elbow region of the Au (111) surface, as shown in Fig. 2(a). After annealed at 550 K, the monomers went through dehalogenation and C–C coupling to form linear precursor chains as displayed in Fig. 2(b). However, in the zoomed-in image in Fig. 2(c), the precursor chains are clearly resolved to be made of short segments as denoted by the red boxes. The chevron stripes are the polymerized backbones, and the bright dots are rotated benzene rings that connect to the backbone with C–C single bonds. Statistics on the length distribution in Fig. 2(g) and Fig. S30 in the ESM display that most precursor chains consist of 2–5 monomers. The limited lengths in this case are most likely due to the steric hindrance imposed by the rotated benzene rings, which prevent the radical addition reactions even though the monomers seem to be close enough.

After further annealed at 700 K, the precursor chains were fully cyclized to form NBN-8-ZGNRs. As shown in Fig. 2(d), most NBN-8-ZGNRs are connected into a branched structure, indicating there were side reactions at 700 K. These side reactions, along with the short precursor backbones yielded in the last step, result in GNRs comprised of few units. Statistics of the length distribution (Fig. 2(g) and Fig. S31 in the ESM) show that about 62% of the products are segments composed of 2 or 3 monomers, while about 18% of them are still monomers. In order to distinguish the boundaries between one-dimensional GNRs and zero-dimensional nanographenes in the products, we used DFT calculated energy gap as a criterion. The calculated DOS of NBN-8-ZGNR segments with increasing number of units reveals that the energy gap decreases with increasing lengths (Fig. S33 in the ESM). The energy gap of tetramer (0.29 eV) is comparable to that of infinite GNR (0.27 eV). Therefore, the nanostructures with more than four monomers can be considered as one-dimensional NBN-8-ZGNRs.

Figure 2(e) displays an NBN-8-ZGNR consisting of 5 monomers. To precisely resolve its structure, we performed nc-AFM imaging in the same area of Fig. 2(e), which clearly shows the zigzag edges. Starting from one terminus of the GNR, we are able to identify the monomers that made up the GNR, as marked by T-shaped boxes in Fig. S34(a) in the ESM. By comparing the atoms along the zigzag edges with those in the BDBT monomer, i.e., the atoms with the same number labels in Figs. S34(a) and S34(b) in the ESM, the NBN motifs can be located along the zigzag edges of NBN-8-ZGNRs. Superimposed with the chemical structure, the NBN motifs are clearly located along the edges, as indicated by the red ovals in Fig. 2(f). Note that there is a bright protrusion at the lower part of the right edge, which, judging from the chemical structure, is a H_2 defect commonly seen in ZGNR edges when using precursors with methyl groups [4].

The two termini of the NBN-8-ZGNR in Fig. 2(f) have different morphologies. The upper terminus (in red shade in Fig. 2(f)) has two protruded benzene rings in the armchair direction, indicating the terminal monomer did not connect with another monomer after dehalogenation. The lower terminus (in yellow shade in Fig. 2(f)) only has one extra benzene ring extending from an armchair ending, which is yielded by the detachment of the α benzene ring. To further understand the termini structures and possible cleavage of bonds during the growth of NBN-8-ZGNRs, more chemical-bond resolved nc-AFM images were obtained, as shown in Fig. 3.

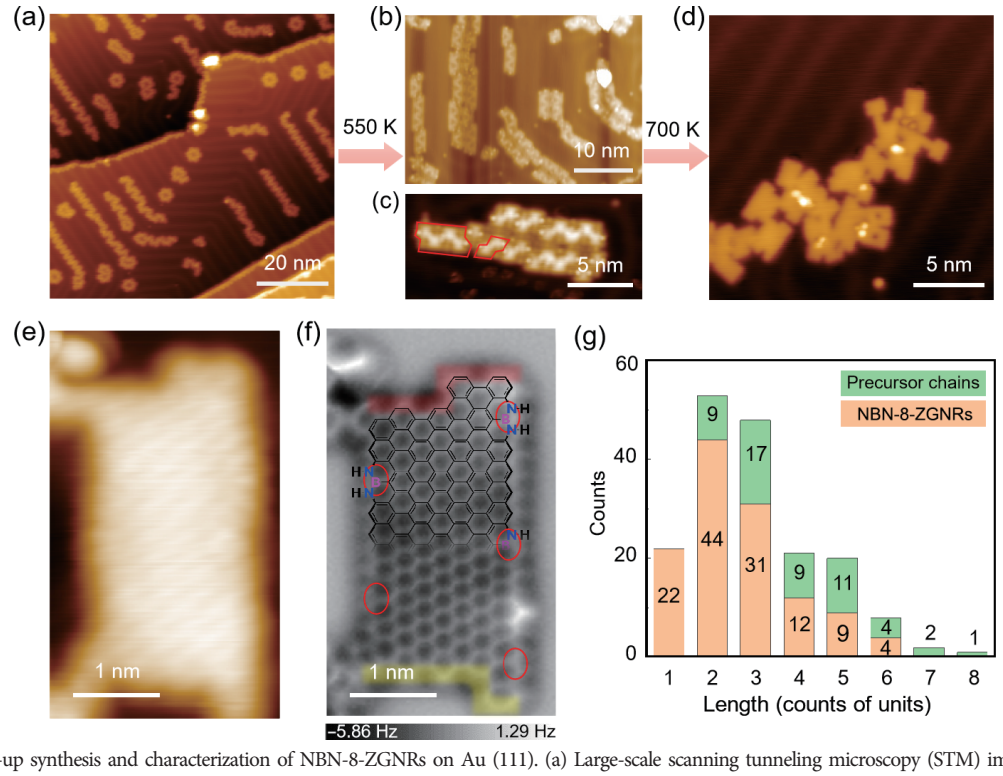

Figure 2 Bottom–up synthesis and characterization of NBN-8-ZGNRs on Au (111). (a) Large-scale scanning tunneling microscopy (STM) image of as-deposited BDBT monomers on Au (111) (the voltage applied on the sample (V_s) = −1 V and the tunneling current (I_t) = 30 pA). (b) Large-scale STM image of precursor chains formed after annealed the sample at 550 K (V_s = −1 V and I_t = 30 pA). (c) High-resolution zoomed-in STM image of the polymers, in which two oligomers are marked by red boxes (V_s = 100 mV and I_t = 50 pA). (d) Large-scale STM image of fully cyclized NBN-8-ZGNRs after annealed the polymers at 700 K (V_s = −200 mV and I_t = 10 pA). (e) Zoomed-in STM image of an NBN-8-ZGNR (V_s = −200 mV and I_t = 40 pA). (f) Constant-height nc-AFM frequency shift image of the ribbon in (e) taken with a CO-functionalized tip. The chemical structure is superimposed on the upper part of the ribbon. The red ovals denote the positions of the NBN motifs. The red and yellow shades denote the upper and lower edges mentioned in the manuscript, respectively. (g) Statistics of the length distribution of the precursor chains (green) and NBN-8-ZGNRs (orange) after annealed at 700 K.

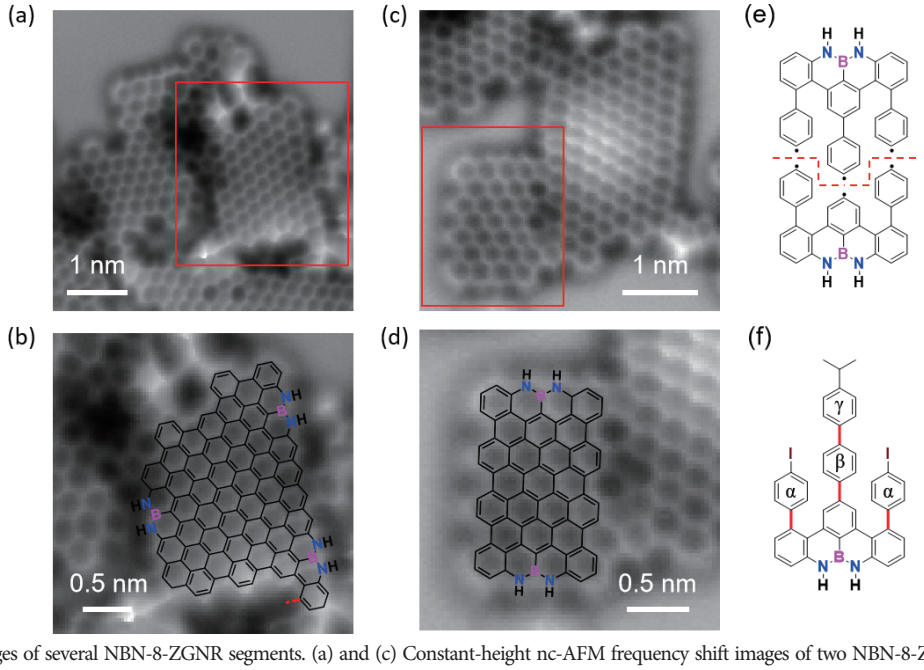

Figure 3 nc-AFM images of several NBN-8-ZGNR segments. (a) and (c) Constant-height nc-AFM frequency shift images of two NBN-8-ZGNR segments. (b) and (d) Zoomed-in images of the red boxes in (a) and (c), respectively, overlayed with chemical structures. The benzene ring in red in (b) signifies the cleavage of an α benzene ring at the terminus. (e) Chemical structures of two monomers in which the C–C bond connecting the β or γ benzene rings is cleaved. The two monomers are separated by a red dashed line. (f) The BDBT molecule structure with the C–C bonds that are most likely to dissociate at elevated temperature labelled in red.

In Figs. 3(a) and 3(b), the same termini are found as those in Fig. 2(f), indicating the detachment of the α benzene ring is easy in the reaction process. The patch in the red box in Fig. 3(c) is another commonly seen structure on the surface. The zoomed-in image in Fig. 3(d) with chemical structure overlayed indicates that this patch is formed by two monomers fused head-to-head, with both β and γ benzene rings cleaved in one monomer and only β benzene ring cleaved in the other, as plotted in Fig. 3(e). From the nc-AFM images, we confirm that the C–C single bonds that connect the α, β, and γ benzene rings are likely to be cleaved during cyclodehydrogenation, as shown in Fig. 3(f) labeled in red, which could be the main reason for the short length and cross-

linked structures of the resulting NBN-8-ZGNRs. Since most precursor chains still contain the α, β, and γ benzene rings as shown in Fig. 2(c), the detachment of these benzene rings should happen at the annealing process of 700 K.

Similar to the case of 6-ZGNRs, there is a strong electronic coupling between NBN-8-ZGNRs and Au (111) surface that suppresses the intrinsic electronic states of the ribbons. As displayed in Fig. S32 in the ESM, the d*I*/d*V* spectra taken on the edges and in the middle of the ribbon are all dominated by the surface states of the gold substrate. In order to decouple the surface states of Au (111), we deposited silicon on the sample and held at 550 K, which leads to the formation of an AuSIL layer on the surface of Au (111), as shown in the inset of Fig. 4(a). The AuSIL strongly changed the morphology of Au (111), on which the herringbone reconstruction transforms to a flat surface. Furthermore, some of the silicon atoms diffuse underneath the ribbons through their edges, which intercalate the AuSIL buffer layer at the interface of NBN-8-ZGNR/Au (111). However, the silicon intercalation also induces contaminations on the NBN-8-ZGNRs, such as residual silicon clusters at the ribbon edges and small silicon (or AuSIL) islands that fill in the interspace of the cross-linked ribbons. The latter case makes it difficult to distinguish the terminus of some ribbons (the black dashed curves in Fig. 4(a)). In addition, the termini of the ribbons seem to be modified by silicon intercalation, transforming the corners between the zigzag and the armchair edges from sharp corners to round corners, as marked by the blue dashed shapes in Fig. 4(a). These modifications indicate that some parts of the ribbons, such as the termini, may be buried under the AuSIL layer.

Figure 4(b) displays a zoomed-in topography of the ribbon in the yellow box in Fig. 4(a). The zigzag edge and the armchair terminus are indicated by red and yellow dashed lines, respectively. Due to the Si clusters attached to one of the edges, Fig. 4(b) only shows the clean zigzag edge of the ribbon. The most likely chemical structure of this ribbon is superimposed in Fig. 4(c). We performed d*I*/d*V* spectra on the zigzag edge (the red and blue dots in Fig. 4(b)) and the interior of the ribbon (the green dot), and the corresponding spectra are shown in Fig. 4(d) in the same color code. The spectrum at the interior of the ribbon nearly mimics that on the AuSIL (the grey spectrum in Fig. 4(d)), only that the density of the occupied states is higher than the unoccupied states. For the spectra at the edge, however, prominent electronic states are observed around Fermi level at −450 and 180 mV, as denoted by P1 and P2 in Fig. 4(d), respectively. DFT calculated DOS on the freestanding model of the structure in Fig. 4(c) exhibits two states around the Fermi level, which can be attributed to the valence band (VB) and conduction band (CB), as displayed in Fig. 4(e). Figures 4(f) and 4(g) demonstrate the spatial distributions of the calculated local DOS at VB and CB, which mainly disperse along the zigzag edges and decay in the interior of the GNR, having the same distributions as the P1 and P2 states obtained in d*I*/d*V* spectra. These results indicate that the electronic states along the edges exist in NBN-8-ZGNRs, and the introduction of the NBN dopants preserves these states and stabilizes the zigzag edges to survive the formation of the AuSIL buffer layer.

3 Conclusions

In conclusion, we have synthesized NBN-8-ZGNRs on Au (111) substrate starting from a specially designed monomer BDBT. nc-

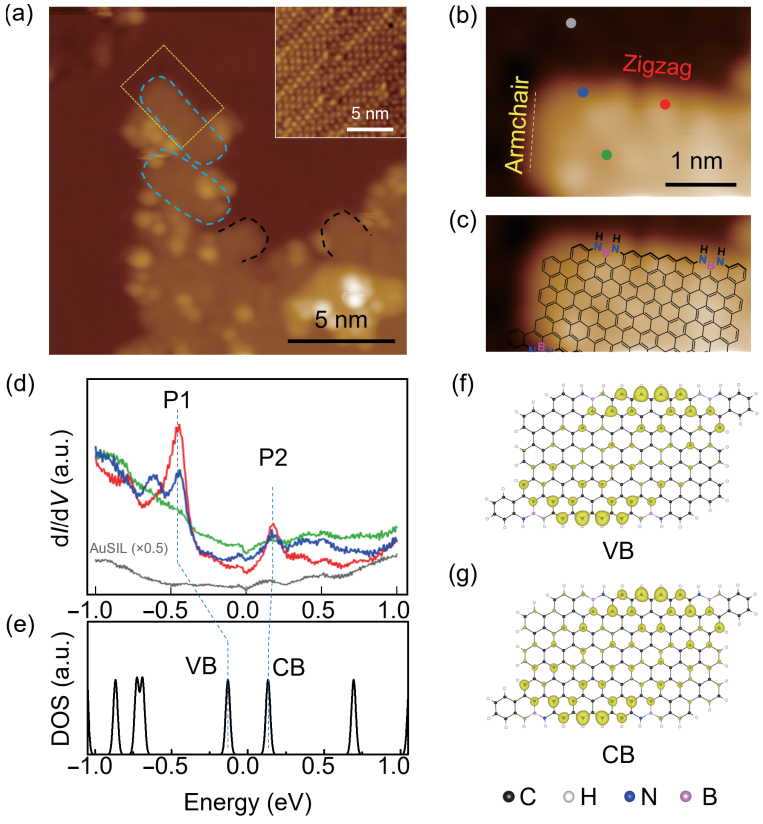

Figure 4 Edge-states characterization of NBN-8-ZGNRs on the Si intercalated Au (111) substrate. (a) Large-scale STM image of NBN-8-ZGNRs on AuSIL/Au (111) (V_s = −1 V and I_t = 50 pA). Blue and black dashed lines indicate the NBN-8-ZGNR segments on AuSIL. The inset is a high-resolution STM image of the AuSIL surface (V_s = −1 V and I_t = 500 pA). (b) Zoomed-in STM image of the ribbon in the yellow box in (a) (V_s = −1 V and I_t = 50 pA). The red and yellow dashed lines indicate the zigzag and armchair edges of the ribbon. The grey, red, blue, and green dots denote the positions where d*I*/d*V* spectra in (d) were performed. (c) Chemical structure superimposed on the same ribbon in (b). (d) d*I*/d*V* spectra obtained on AuSIL substrate (grey), GNR zigzag edge (red and blue), and GNR interior (green) (V_s = −1 V and I_t = 1 nA before opening feedback loop, frequency = 931 Hz, and the modulation amplitude (V_{mod}) = 5 mV). (e) DFT calculated DOS. Spatial distributions of local DOS at (f) VB and (g) CB of a freestanding NBN-8-ZGNR segment.

AFM images confirm the successful introduction of a NBN dopant superlattice along the zigzag edges, and reveal that the additional benzene rings are easy to detach from the NBN core, which results in short segments of NBN-8-ZGNRs. After the formation of AuSIL buffer layer, the ribbons are electronically decoupled from the substrate, enabling us to detect the edge states. Our work provides a new ribbon with NBN dopants and a larger width in the ZGNR toolbox compared with the existing ones, and reveals that the zigzag edges in NBN-8-ZGNRs are robust enough to survive the formation of AuSIL at the ZGNR/Au (111) interface.

Acknowledgements

The work was supported by grants from the National Key Research and Development Program of China (No. 2019YFA0308500), the National Natural Science Foundation of China (No. 61888102), the Chinese Academy of Sciences (Nos. XDB30000000 and YSBR-003), the EU Graphene Flagship (Graphene Core 3, No. 881603), the H2020-MSCA-ITN (ULTIMATE, No. 813036), the Center for Advancing Electronics Dresden (CfAED), the H2020-EU.1.2.2.-FET Proactive Grant (LIGHT-CAP, No. 101017821), and the DFG-SNSF Joint Switzerland-German Research Project (EnhanTopo, No. 429265950).

Electronic Supplementary Material: Supplementary material (additional information on precursor synthesis route, NMR spectra and mass spectroscopy measurements, and GNR statistics based on STM images) is available in the online version of this article at https://doi.org/10.1007/s12274-023-5605-2.

References

[1] Han, W.; Kawakami, R. K.; Gmitra, M.; Fabian, J. Graphene spintronics. *Nat. Nanotechnol.* **2014**, *9*, 794–807.

[2] Nakada, K.; Fujita, M.; Dresselhaus, G.; Dresselhaus, M. S. Edge state in graphene ribbons: Nanometer size effect and edge shape dependence. *Phys. Rev. B* **1996**, *54*, 17954–17961.

[3] Han, P.; Akagi, K.; Canova, F. F.; Mutoh, H.; Shiraki, S.; Iwaya, K.; Weiss, P. S.; Asao, N.; Hitosugi, T. Bottom–up graphene-nanoribbon fabrication reveals chiral edges and enantioselectivity. *ACS Nano* **2014**, *8*, 9181–9187.

[4] Ruffieux, P.; Wang, S. Y.; Yang, B.; Sánchez-Sánchez, C.; Liu, J.; Dienel, T.; Talirz, L.; Shinde, P.; Pignedoli, C. A.; Passerone, D. et al. On-surface synthesis of graphene nanoribbons with zigzag edge topology. *Nature* **2016**, *531*, 489–492.

[5] Talirz, L.; Söde, H.; Dumslaff, T.; Wang, S. Y.; Sanchez-Valencia, J. R.; Liu, J.; Shinde, P.; Pignedoli, C. A.; Liang, L. B.; Meunier, V. et al. On-surface synthesis and characterization of 9-atom wide armchair graphene nanoribbons. *ACS Nano* **2017**, *11*, 1380–1388.

[6] Gröning, O.; Wang, S. Y.; Yao, X. L.; Pignedoli, C. A.; Barin, G. B.; Daniels, C.; Cupo, A.; Meunier, V.; Feng, X. L.; Narita, A. et al. Engineering of robust topological quantum phases in graphene nanoribbons. *Nature* **2018**, *560*, 209–213.

[7] Rizzo, D. J.; Veber, G.; Cao, T.; Bronner, C.; Chen, T.; Zhao, F. Z.; Rodriguez, H.; Louie, S. G.; Crommie, M. F.; Fischer, F. R. Topological band engineering of graphene nanoribbons. *Nature* **2018**, *560*, 204–208.

[8] Rizzo, D. J.; Veber, G.; Jiang, J. W.; McCurdy, R.; Cao, T.; Bronner, C.; Chen, T.; Louie, S. G.; Fischer, F. R.; Crommie, M. F. Inducing metallicity in graphene nanoribbons via zero-mode superlattices. *Science* **2020**, *369*, 1597–1603.

[9] Cai, J. M.; Ruffieux, P.; Jaafar, R.; Bieri, M.; Braun, T.; Blankenburg, S.; Muoth, M.; Seitsonen, A. P.; Saleh, M.; Feng, X. L. et al. Atomically precise bottom–up fabrication of graphene nanoribbons. *Nature* **2010**, *466*, 470–473.

[10] Liu, J. Z.; Li, B. W.; Tan, Y. Z.; Giannakopoulos, A.; Sanchez-Sanchez, C.; Beljonne, D.; Ruffieux, P.; Fasel, R.; Feng, X. L.; Müllen, K. Toward cove-edged low band gap graphene nanoribbons. *J. Am. Chem. Soc.* **2015**, *137*, 6097–6103.

[11] Senkovskiy, B. V.; Usachov, D. Y.; Fedorov, A. V.; Marangoni, T.; Haberer, D.; Tresca, C.; Profeta, G.; Caciuc, V.; Tsukamoto, S.; Atodiresei, N. et al. Boron-doped graphene nanoribbons: Electronic structure and Raman fingerprint. *ACS Nano* **2018**, *12*, 7571–7582.

[12] Sun, K. W.; Silveira, O. J.; Saito, S.; Sagisaka, K.; Yamaguchi, S.; Foster, A. S.; Kawai, S. Manipulation of spin polarization in boron-substituted graphene nanoribbons. *ACS Nano* **2022**, *16*, 11244–11250.

[13] Cloke, R. R.; Marangoni, T.; Nguyen, G. D.; Joshi, T.; Rizzo, D. J.; Bronner, C.; Cao, T.; Louie, S. G.; Crommie, M. F.; Fischer, F. R. Site-specific substitutional boron doping of semiconducting armchair graphene nanoribbons. *J. Am. Chem. Soc.* **2015**, *137*, 8872–8875.

[14] Blackwell, R. E.; Zhao, F. Z.; Brooks, E.; Zhu, J. M.; Piskun, I.; Wang, S. K.; Delgado, A.; Lee, Y. L.; Louie, S. G.; Fischer, F. R. Spin splitting of dopant edge state in magnetic zigzag graphene nanoribbons. *Nature* **2021**, *600*, 647–652.

[15] Cao, Y.; Qi, J.; Zhang, Y. F.; Huang, L.; Zheng, Q.; Lin, X.; Cheng, Z. H.; Zhang, Y. Y.; Feng, X. L.; Du, S. X. et al. Tuning the morphology of chevron-type graphene nanoribbons by choice of annealing temperature. *Nano Res.* **2018**, *11*, 6190–6196.

[16] Liu, X. M.; Li, G.; Lipatov, A.; Sun, T.; Mehdi Pour, M.; Aluru, N. R.; Lyding, J. W.; Sinitskii, A. Chevron-type graphene nanoribbons with a reduced energy band gap: Solution synthesis, scanning tunneling microscopy, and electrical characterization. *Nano Res.* **2020**, *13*, 1713–1722.

[17] Cai, J. M.; Pignedoli, C. A.; Talirz, L.; Ruffieux, P.; Söde, H.; Liang, L. B.; Meunier, V.; Berger, R.; Li, R. J.; Feng, X. L. et al. Graphene nanoribbon heterojunctions. *Nat. Nanotechnol.* **2014**, *9*, 896–900.

[18] Pawlak, R.; Liu, X. S.; Ninova, S.; D'Astolfo, P.; Drechsel, C.; Sangtarash, S.; Häner, R.; Decurtins, S.; Sadeghi, H.; Lambert, C. J. et al. Bottom–up synthesis of nitrogen-doped porous graphene nanoribbons. *J. Am. Chem. Soc.* **2020**, *142*, 12568–12573.

[19] Wen, E. C. H.; Jacobse, P. H.; Jiang, J. W.; Wang, Z. Y.; McCurdy, R. D.; Louie, S. G.; Crommie, M. F.; Fischer, F. R. Magnetic interactions in substitutional core-doped graphene nanoribbons. *J. Am. Chem. Soc.* **2022**, *144*, 13696–13703.

[20] Kawai, S.; Saito, S.; Osumi, S.; Yamaguchi, S.; Foster, A. S.; Spijker, P.; Meyer, E. Atomically controlled substitutional boron-doping of graphene nanoribbons. *Nat. Commun.* **2015**, *6*, 8098.

[21] Yang, H.; Gao, Y. X.; Niu, W. H.; Chang, X.; Huang, L.; Liu, J. Z.; Mai, Y.; Feng, X. L.; Du, S. X.; Gao, H. J. Fabrication of sulfur-doped cove-edged graphene nanoribbons on Au (111). *Chin. Phys. B* **2021**, *30*, 077306.

[22] Nguyen, G. D.; Toma, F. M.; Cao, T.; Pedramrazi, Z.; Chen, C.; Rizzo, D. J.; Joshi, T.; Bronner, C.; Chen, Y. C.; Favaro, M. et al. Bottom–up synthesis of $N = 13$ sulfur-doped graphene nanoribbons. *J. Phys. Chem. C* **2016**, *120*, 2684–2687.

[23] Chen, Y. C.; Cao, T.; Chen, C.; Pedramrazi, Z.; Haberer, D.; De Oteyza, D. G.; Fischer, F. R.; Louie, S. G.; Crommie, M. F. Molecular bandgap engineering of bottom–up synthesized graphene nanoribbon heterojunctions. *Nat. Nanotechnol.* **2015**, *10*, 156–160.

[24] Senkovskiy, B. V.; Nenashev, A. V.; Alavi, S. K.; Falke, Y.; Hell, M.; Bampoulis, P.; Rybkovskiy, D. V.; Usachov, D. Y.; Fedorov, A. V.; Chernov, A. I. et al. Tunneling current modulation in atomically precise graphene nanoribbon heterojunctions. *Nat. Commun.* **2021**, *12*, 2542.

[25] Rizzo, D. J.; Wu, M.; Tsai, H. Z.; Marangoni, T.; Durr, R. A.; Omrani, A. A.; Liou, F.; Bronner, C.; Joshi, T.; Nguyen, G. D. et al. Length-dependent evolution of type II heterojunctions in bottom–up-synthesized graphene nanoribbons. *Nano Lett.* **2019**, *19*, 3221–3228.

[26] Nguyen, G. D.; Tsai, H. Z.; Omrani, A. A.; Marangoni, T.; Wu, M.; Rizzo, D. J.; Rodgers, G. F.; Cloke, R. R.; Durr, R. A.; Sakai, Y. et al. Atomically precise graphene nanoribbon heterojunctions from a single molecular precursor. *Nat. Nanotechnol.* **2017**, *12*, 1077–1082.

[27] Li, J. C.; Sanz, S.; Merino-Díez, N.; Vilas-Varela, M.; Garcia-Lekue, A.; Corso, M.; De Oteyza, D. G.; Frederiksen, T.; Peña, D.; Pascual, J. I. Topological phase transition in chiral graphene nanoribbons:

From edge bands to end states. *Nat. Commun.* **2021**, *12*, 5538.
[28] Guo, G. P.; Lin, Z. R.; Tu, T.; Cao, G.; Li, X. P.; Guo, G. C. Quantum computation with graphene nanoribbon. *New J. Phys.* **2009**, *11*, 123005.
[29] Luis, F.; Coronado, E. Spinning on the edge of graphene. *Nature* **2018**, *557*, 645–647.
[30] Mandal, B.; Sarkar, S.; Pramanik, A.; Sarkar, P. Doped defective graphene nanoribbons: A new class of materials with novel spin filtering properties. *RSC Adv.* **2014**, *4*, 49946–49952.
[31] Berdonces-Layunta, A.; Lawrence, J.; Edalatmanesh, S.; Castro-Esteban, J.; Wang, T.; Mohammed, M. S. G.; Colazzo, L.; Peña, D.; Jelínek, P.; De Oteyza, D. G. Chemical stability of (3,1)-chiral graphene nanoribbons. *ACS Nano* **2021**, *15*, 5610–5617.
[32] Lawrence, J.; Berdonces-Layunta, A.; Edalatmanesh, S.; Castro-Esteban, J.; Wang, T.; Jimenez-Martin, A.; De La Torre, B.; Castrillo-Bodero, R.; Angulo-Portugal, P.; Mohammed, M. S. G. et al. Circumventing the stability problems of graphene nanoribbon zigzag edges. *Nat. Chem.* **2022**, *14*, 1451–1458.
[33] Fu, Y. B.; Yang, H.; Gao, Y. X.; Huang, L.; Berger, R.; Liu, J. Z.; Lu, H. L.; Cheng, Z. H.; Du, S. X.; Gao, H. J. et al. On-surface synthesis of NBN-doped zigzag-edged graphene nanoribbons. *Angew. Chem., Int. Ed.* **2020**, *132*, 8958–8964.
[34] Fu, Y. B.; Chang, X.; Yang, H.; Dmitrieva, E.; Gao, Y. X.; Ma, J.; Huang, L.; Liu, J. Z.; Lu, H. L.; Cheng, Z. H. et al. NBN-doped bis-tetracene and peri-tetracene: Synthesis and characterization. *Angew. Chem., Int. Ed.* **2021**, *60*, 26115–26121.
[35] Wang, X. Y.; Zhang, F.; Schellhammer, K. S.; Machata, P.; Ortmann, F.; Cuniberti, G.; Fu, Y. B.; Hunger, J.; Tang, R. Z.; Popov, A. A. et al. Synthesis of NBN-type zigzag-edged polycyclic aromatic hydrocarbons: 1,9-Diaza-9a-boraphenalene as a structural motif. *J. Am. Chem. Soc.* **2016**, *138*, 11606–11615.
[36] Mao, J. H.; Huang, L.; Pan, Y.; Gao, M.; He, J. F.; Zhou, H. T.; Guo, H. M.; Tian, Y.; Zou, Q.; Zhang, L. Z. et al. Silicon layer intercalation of centimeter-scale, epitaxially grown monolayer graphene on Ru (0001). *Appl. Phys. Lett.* **2012**, *100*, 093101.
[37] Li, G.; Zhou, H. T.; Pan, L. D.; Zhang, Y.; Huang, L.; Xu, W. Y.; Du, S. X.; Ouyang, M.; Ferrari, A. C.; Gao, H. J. Role of cooperative interactions in the intercalation of heteroatoms between graphene and a metal substrate. *J. Am. Chem. Soc.* **2015**, *137*, 7099–7103.
[38] Guo, H.; Wang, X. Y.; Huang, L.; Jin, X.; Yang, Z. Z.; Zhou, Z.; Hu, H.; Zhang, Y. Y.; Lu, H. L.; Zhang, Q. H. et al. Insulating SiO_2 under centimeter-scale, single-crystal graphene enables electronic-device fabrication. *Nano Lett.* **2020**, *20*, 8584–8591.
[39] Deniz, O.; Sánchez-Sánchez, C.; Dumslaff, T.; Feng, X. L.; Narita, A.; Müllen, K.; Kharche, N.; Meunier, V.; Fasel, R.; Ruffieux, P. Revealing the electronic structure of silicon intercalated armchair graphene nanoribbons by scanning tunneling spectroscopy. *Nano Lett.* **2017**, *17*, 2197–2203.